PROCEEDINGS A

rspa.royalsocietypublishing.org

Research

Article submitted to journal

Subject Areas:
applied mathematics, fluid dynamics, aerodynamics

Keywords:
riemann-hilbert, singular integral equation, aerofoil design

Author for correspondence:
P. J. Baddoo
e-mail: baddoo@damtp.cam.ac.uk

Potential Flow through a Cascade of Aerofoils: Direct and Inverse Problems

P. J. Baddoo and L. J. Ayton

Department of Applied Mathematics and Theoretical Physics, Wilberforce Road, Cambridge, CB3 0WA.

The potential flow through an infinite cascade of aerofoils is considered as both a direct and inverse problem. In each case, a perturbation expansion about a background uniform flow is assumed where the size of the perturbation is comparable to the aspect ratio of the aerofoils. This perturbation must decay far upstream and also satisfy particular edge conditions, including the Kutta condition at each trailing edge. In the direct problem, the flow field through a cascade of aerofoils of known geometry is calculated. This is solved analytically by recasting the situation as a Riemann-Hilbert problem with only imaginary values prescribed on the chords. As the distance between aerofoils is taken to infinity, the solution is seen to converge to a known analytic expression for a single aerofoil. Analytic expressions for the surface velocity, lift, and deflection angle are presented as functions of aerofoil geometry, angle of attack and stagger angle; these show good agreement with numerical results. In the inverse problem, the aerofoil geometry is calculated from a prescribed tangential surface velocity along the chords and upstream angle of attack. This is found via the solution of a singular integral equation prescribed on the chords of the aerofoils.

1. Introduction

Potential flow past a periodic array of bodies is commonplace in a large range of fluid mechanical problems. For example; the flow through a rotor cascade in aerodynamics [17], the flow through structured porous materials [6], and the flow around large schools of fish [20]. Within these applications it is not merely the potential flow through the structure that must be calculated but also the complicated interactions between unsteady perturbations to the flow (such as turbulence) and the structures themselves. To approach any of these

THE ROYAL SOCIETY PUBLISHING

complex unsteady interactions it is vital to have a clear understanding of the background steady flow as it can convect and distort the unsteady perturbations. However, there is a distinct lack of analytic solutions for uniform flow past periodic arrays.

Early research [3] considers the uniform flow past an array of cylinders which have small diameters compared to their separation distance through the use of asymptotic analysis. The development of a novel transform method known formally as the Unified Transform Method [12] (but more commonly as the Fokas method) allowed Crowdy [9] to extend Balsa's work [3] to allow for arbitrary ratios of diameter to separation distance. By solving the problem of uniform flow around cylinders, one could perhaps use a conformal mapping from a periodic array of non-cylindrical structures, to the cylindrical array described by Crowdy [9]. Unfortunately, these mappings are often impossible to invert analytically and thus a numerical scheme must be implemented [25].

Although there are already several ways to calculate the potential flow through a cascade of aerofoils, analytical solutions that elucidate the underlying physics are rare. One well-known solution for flat plates at angle of attack can be found by constructing a conformal map from a canonical circular domain to the cascade [22, p. 149]. Whilst this solution is exact, the expression for the conformal mapping is not invertible, so the velocity field may only be written implicitly. Another method that is ubiquitous in thin-aerofoil theory is the method of singularities: the rigid aerofoil surface is modelled as a distribution of mass sources and vortices on the chord (for thin aerofoils) or the surface (for thick aerofoils). This theory has been applied to cascades on several occasions [11,23,24], the latter of which is only valid for large chord-to-gap ratios. The vortex distribution is typically written as a Glauert sine series, which corresponds to a series of weighted Chebyshev polynomials in physical space. These methods (of conformal mappings and Glauert sine series) have been combined [10] to provide an analytical expression for the steady flow near the leading edges.

This paper therefore presents a new solution, based on solving a Riemann-Hilbert problem [21], for the potential flow through a periodic array of structures. We focus on applications towards aerodynamics and biological swimming and consequently consider situations where the structures are formally thin (the vertical height of the structure is much smaller than the horizontal length). By imposing this asymptotic condition, great analytic progress can be achieved, as in the case of Balsa [3]. Specifically, we shall consider a periodic array, or cascade, of aerofoils. We do so for two reasons; firstly, these are the most common shapes associated with aerodynamics and biological swimming, and, secondly, these allow us to consider the effects of a sharp trailing edge of the rigid body (something not accounted for by cylinders). The sharp trailing edge requires imposition of a Kutta condition, which ensures the flow leaves the trailing edge smoothly. Our analysis will however also be valid for thin bodies that do not require a Kutta condition (i.e. do not have sharp edges) such as ellipses.

In addition to the *direct* problem, of obtaining the potential flow through a cascade of aerofoils with specified geometry, this approach allows us to also solve the *inverse* problem: given a desired flow around an aerofoil within the cascade, we can determine the geometry of each aerofoil within the cascade required to generate this specific flow. The specification of tangential velocity is essential in blade design for axial-flow compressors in order to control boundary-layer growth and separation [14].

The layout of this paper is as follows: in Section 2 we set up the Riemann-Hilbert problem for the potential flow through a cascade of aerofoils. In Section 3 we solve the direct problem by segregating the boundary conditions arising due to thickness, camber and angle of attack, and in Section 4 we use equations derived in the direct problem to solve the inverse problem. In Section 5 we present results for the potential flow through cascades of aerofoils for a variety of geometries and angles of attack. We show the analytic solution is useful for calculating key parameters associated to the flow, such as surface velocity, lift, and deflection angle. We also demonstrate the inverse problem for a particular class of aerofoil geometries. Finally, in Section 6 we discuss the conclusions of the paper.

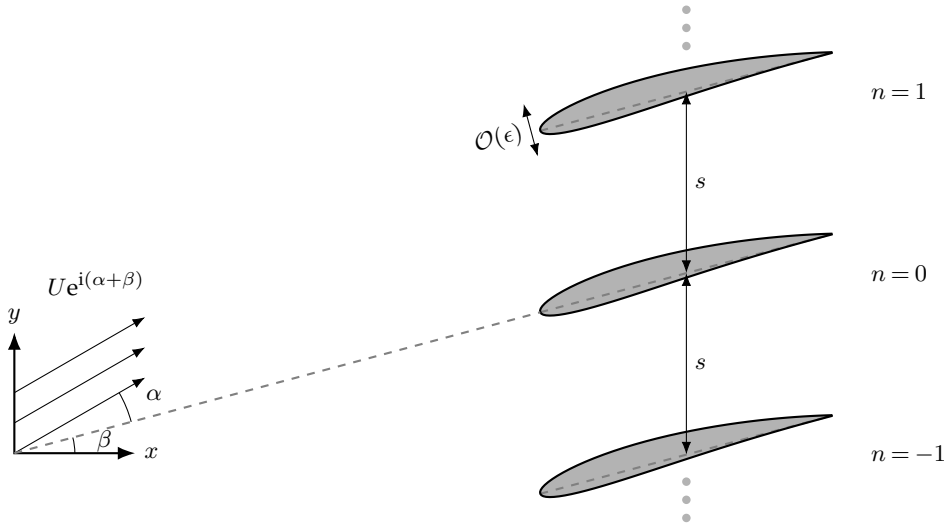

Figure 1: A infinite, staggered cascade of aerofoils. The vertical spacing between the aerofoils is s, and the upstream velocity is U, which is inclined at angle of attack α.

2. Model Derivation

Consider an infinite cascade of thin aerofoils under the assumption of small disturbances in a two-dimensional, steady, incompressible flow. We non-dimensionalise lengths so that the semi-chord of each aerofoil is 1. The extension to compressible flows may be achieved via a Prandtl-Glauert transformation [19]. The flow is uniform far upstream and has angle of attack α relative to the chords of the aerofoils, which are inclined at stagger angle β. We assume that $\alpha,\ \beta = \mathcal{O}(\epsilon)$ where ϵ is a small parameter the order of the aspect ratio of the aerofoils. This arrangement is illustrated in figure 1. We write the complex potential for the total steady flow in the form of a series expansion in ϵ:

$$w(z) = U\left(z e^{-i(\alpha+\beta)} + \epsilon\, w_1(z) + \mathcal{O}(\epsilon^2)\right),$$

where $z = x + iy$ and $w_1(z)$ is a function to be found subject to a no-flux boundary condition on the aerofoils' surfaces, appropriate edge conditions at the leading and trailing edges, and decay far upstream.

We denote the upper and lower boundaries of the n^{th} aerofoil as $y^{\pm}_{b,n}(t)$ respectively, so that

$$y^{\pm}_{b,n}(t) = \epsilon y^{\pm}_{b}(t) + t\sin(\beta) + ins,$$

and $y^{\pm}_{b}(t) = \pm y_{th}(t) + y_c(t)$, where the subscripts th and c denote thickness and camber respectively, $n \in \mathbb{Z}$ and $t \in [-1, 1]$ parametrises the aerofoil chord. We restrict our analysis to bodies that have, at worst, parabolic noses, i.e. $y_{th} \sim \sqrt{t}$ as $t \to -1$. This is in line with the NACA 4-digit aerofoil series that is commonplace in the literature. Any trailing edge angle is permitted by the analysis, including cusped ends and finite angle trailing edges. In the latter case, we expect a stagnation point to form at the trailing edge. This can be proved via a conformal mapping for a semi-infinite wedge [4, p. 412]. In practice, this means that our perturbation solution will have a log singularity at the trailing edge to create a stagnation point when combined with the $\mathcal{O}(1)$ solution. Additionally, we require that $y^{\pm\prime}_{b}(t)$ satisfies a Hölder condition on $t \in (-1, 1)$.

The no-flux boundary condition requires $\partial\,\mathrm{Re}[w]/\partial n = 0$ on the boundary of the aerofoil, except at the sharp trailing edge where the outward normal derivative is undefined. Since the outward normal to the upper (lower) surface of each aerofoil is given by $(-\epsilon y^{\pm\prime}_{b,n}(t), 1)$, the no-flux

condition on the upper (lower) surface is $(-\epsilon y_{b,n}^{\pm\prime}, 1) \cdot \nabla \operatorname{Re}[w] = 0$, i.e.

$$0 = \left(-y_b^{\pm\prime}(t), 1\right) \cdot \left(1 + \epsilon u^{\pm}(t)\ , (\alpha+\beta) + \epsilon v^{\pm}(t)\right) + \mathcal{O}(\epsilon^2) \tag{2.1}$$

$$= -y_b^{\pm\prime}(t) + (\alpha+\beta) + \epsilon v^{\pm}(t) + \mathcal{O}(\epsilon^2), \tag{2.2}$$

where we have assumed that $y_b^{\pm\prime}$, $u^{\pm}$, $v^{\pm}$ are all $\mathcal{O}(1)$. This assumption proves to be valid everywhere except in an $\mathcal{O}(\epsilon^2)$ region close to the leading edge where a further asymptotic expansion would be required, however this is beyond the scope of this paper.

Since $\epsilon \ll 1$, we can use Taylor's theorem to apply the no-flux condition on the aerofoils' surface to their chords. Furthermore, since β is small, we may approximate the staggered chord as a chord with no stagger. This approximation has an $\mathcal{O}(\epsilon^2)$ effect on the solution, and will be inverted at the end of Section 3 in order to properly locate the leading and trailing edge stagnation points. Accordingly, we may write analytic, periodic f,

$$\epsilon f(t, y_{b,n}^{\pm}(t)) = \epsilon f^{\pm}(t) + \mathcal{O}(\epsilon^2). \tag{2.3}$$

Combining (2.2) and (2.3) yields

$$\epsilon v(t, ins\pm) = y_{b,n}^{\pm\prime}(t) - \alpha - \beta = \epsilon y_c'(t) - \alpha \pm \epsilon y_{th}'(t). \tag{2.4}$$

The superscript $\pm$ here indicates the limiting value taken on the upper and lower sides of L respectively, where L is defined as the union of the unstaggered chords traversed from leading edge to trailing edge. Hence, by considering the complex velocity $\Phi(z) = w'(z) = u(x,y) - \mathrm{i}v(x,y)$ either side of L, Φ must satisfy

$$\Phi^{\pm}(t) = u^{\pm}(t) - \mathrm{i}\left(y_c'(t) - \alpha \pm y_{th}'(t)\right), \tag{2.5}$$

where $u^{\pm}$ are the unknown upper and lower tangential surface velocities. If we can solve for $\Phi(z)$, we can obtain the tangential surface velocities and the total complex potential, $w(z)$.

In addition to the no-flux condition, we must also enforce the Kutta condition and set the circulation such that the rear stagnation point is located at the trailing edge of the aerofoils. This is equivalent to specifying that the flows over the upper and lower surfaces are parallel to one another at the trailing edge [8]. Since this formulation does not permit any wakes, it is sufficient to impose the jump in tangential velocity to be zero at the trailing edge. At the leading edge, thin aerofoil theory [1] tells us that the fluid velocity scales as the inverse square root of the distance from the leading edge, so we permit square root singularities here. To fully summarise our problem, we are seeking a function $\Phi(z)$ such that

(I) $\Phi(z)$ satisfies Laplace's equation (is holomorphic) in $\mathbb{C} \setminus \overline{L}$,
(II) The boundary conditions in (2.5) are satisfied either side of L,
(III) $\Phi(z) = \mathcal{O}\left(|z|^{-1/2}\right)$ as z approaches the leading edge of each aerofoil,
(IV) $\Phi(t)$ has zero jump in tangential velocity as t approaches the trailing edge along the chord, and,
(V) $\Phi(z) \to 0$ as $z \to -\infty$.

Once we know $\Phi(z)$ we can obtain the potential flow around the cascade correct to $\mathcal{O}(\epsilon)$. In the following section, we find a solution by modelling (I-V) as a Riemann-Hilbert problem.

3. Direct Problem Solution

We seek to solve (I–V) as a Riemann-Hilbert problem [21] but must first note several non-standard features of the formulation. First, the contour L is unbounded, and is an infinite union of disjoint contours. Much of the analysis of Riemann-Hilbert problems is only applicable to problems defined on bounded, finite contours. However, we do not require all of the theory to solve this problem, and show in Appendix A that, due to the periodicity of the problem, there is a modified

form of the Plemelj formulae (6.3) which may be applied in this case. This modified form is used to find the "density function" and solve (I, II) in 3(a). Due to the periodicity, one part of the theory that we cannot recover is the restriction that the Cauchy type integral $\Phi \to 0$ as $|z| \to \infty$, but the use of a fundamental solution in 3(b) is sufficient to fix the upstream behaviour for (V). Additionally, key asymptotic results at the endpoints, given in Appendix B, may also be recovered and can be used to check the edge conditions (III, IV) in 3(c).

A second non-standard feature of the problem is that only the imaginary data is prescribed on L, as opposed to the full value of Φ. The unknown real data $u^{\pm}(t)$ may be removed by employing the Schwarz reflection principle [2, p. 346]. We write the complex velocity as

$$\Phi(z) = \Phi_{th}(z) + \Phi_{c,\alpha}(z),$$

where

$$\Phi_{th}(z) = \frac{1}{2}\left(\Phi(z) + \overline{\Phi}(z)\right), \qquad \Phi_{c,\alpha}(z) = \frac{1}{2}\left(\Phi(z) - \overline{\Phi}(z)\right). \tag{3.1}$$

The overline " – " denotes the Schwarz conjugate (denoted in [2] as "$\sim$"). These functions have the properties

$$\Phi_{th}(z) = \overline{\Phi}_{th}(z), \qquad \Phi_{c,\alpha}(z) = -\overline{\Phi}_{c,\alpha}(z).$$

By taking the limiting value of Φ either side of L, we obtain

$$\Phi^{+}_{th}(t) - \Phi^{-}_{th}(t) = -2\mathrm{i}y'_{th}(t), \tag{3.2}$$

$$\Phi^{+}_{c,\alpha}(t) + \Phi^{-}_{c,\alpha}(t) = -2\mathrm{i}y'_{c}(t) + 2\mathrm{i}\alpha, \tag{3.3}$$

which are two Riemann-Hilbert problems. This formulation yields convenient boundary values on the chords that only take known imaginary values on L and unknown real quantities, $u^{\pm}(t)$, have been removed.

(a) General Solution

Here we find the general solution for Φ, satisfying (I, II) which we will later modify to set the upstream behaviour and satisfy the edge conditions (III, IV, V). We treat the thickness, camber, and angle of attack problems separately since the boundary condition is linear.

(i) Thickness Term, Φ_{th}

Here we solve (3.2). This is a straightforward Riemann-Hilbert problem and the solution is

$$\Phi_{th}(z) = \frac{1}{2\pi\mathrm{i}} \int_{L} \frac{-2\mathrm{i}y'_{th}(\tau)}{\tau - z}\, \mathrm{d}\tau, \tag{3.4}$$

which can easily be verified with the Modified Plemelj Formulae (6.3). We use the result (6.1) from Appendix A to write

$$\Phi_{th}(z) = -\frac{1}{s}\int_{-1}^{1} y'_{th}(\tau) \coth\left(\frac{\pi(\tau - z)}{s}\right) \mathrm{d}\tau. \tag{3.5}$$

(ii) Camber Term, Φ_c

Now we solve for the camber term by splitting $\Phi_{c,\alpha}$ into terms dependant on angle of attack and camber. We decompose (3.3) into parts depending only on camber and write

$$\Phi^{+}_{c}(t) + \Phi^{-}_{c}(t) = -2\mathrm{i}y'_{c}(t). \tag{3.6}$$

The solution to this type of Riemann-Hilbert problem for bounded contours is detailed in [13, p. 429]. This solution relied on constructing a bounded, closed contour that connects the contours along which the Riemann-Hilbert problem is defined. This is not possible in our case, but the

method may be adapted. We first need to solve the homogeneous equation to find the so-called fundamental solution, which we denote by $X(z)$. In general, the homogeneous equation is

$$X^+(t) = G(t)X^-(t),$$

and a solution is given by [13, 43.2] as

$$X(z) = \mathrm{e}^{\Pi(z)}, \qquad \Pi(z) = \frac{1}{2\pi\mathrm{i}}\int_L \frac{\log G(\tau)}{\tau - z}\mathrm{d}\tau.$$

In our case, the homogeneous equation is

$$X^+(t) + X^-(t) = 0,$$

and we have $\log(G) = \pi\mathrm{i}(1+2n)$. Therefore,

$$\Pi(z) = \left(n+\frac{1}{2}\right)\int_L \frac{1}{\tau - z}\mathrm{d}\tau = \left(n+\frac{1}{2}\right)\log\left(\frac{\sinh\left(\frac{\pi(z-1)}{s}\right)}{\sinh\left(\frac{\pi(z+1)}{s}\right)}\right).$$

More solutions to the homogeneous equation may be found by multiplying or dividing by polynomials whose the roots are the endpoints of the contours. This is useful when specifying whether the behaviour at either endpoint is permitted to be unbounded. In the periodic case, this non-uniqueness of solutions can be expressed as

$$\begin{aligned} X(z) &= \left[\sinh\left(\frac{\pi(z+1)}{s}\right)\right]^{\lambda}\left[\sinh\left(\frac{\pi(z-1)}{s}\right)\right]^{\mu}\mathrm{e}^{\Pi(z)} \\ &= \left[\sinh\left(\frac{\pi(z+1)}{s}\right)\right]^{\lambda-n-\frac{1}{2}}\left[\sinh\left(\frac{\pi(z-1)}{s}\right)\right]^{\mu+n+\frac{1}{2}}, \end{aligned}$$

where λ and μ are integers chosen to satisfy

$$-1 < \lambda - n - \frac{1}{2} < 1, \qquad -1 < \mu + n + \frac{1}{2} < 1.$$

At this point we recall the conditions on the endpoint behaviour needed to satisfy the Kutta condition and leading edge behaviour. There are two choices each for λ and μ but we choose $\lambda = n$, $\mu = -n$ in order to satisfy (III) and (IV). We choose the branch connecting the branch points at the leading and trailing edges. Therefore,

$$X(z) = \sqrt{\frac{\sinh\left(\frac{\pi(z-1)}{s}\right)}{\sinh\left(\frac{\pi(z+1)}{s}\right)}},$$

and the limiting value either side of L, with this choice of branch, is

$$X^{\pm}(t) = \pm\mathrm{i}\sqrt{\frac{\sinh\left(\frac{\pi(1-t)}{s}\right)}{\sinh\left(\frac{\pi(1+t)}{s}\right)}}.$$

Following [13], we now use the fundamental solution to solve the inhomogeneous problem. We write

$$\Phi_c(z) = X(z)\Psi(z),$$

so that Ψ satisfies

$$\Psi^+(t) - \Psi^-(t) = -\frac{2\mathrm{i}y_c'(t)}{X^+(t)}.$$

This is a Riemann-Hilbert problem of the form (3.5) and has solution

$$\Psi(z) = \frac{1}{2\pi\mathrm{i}}\int_L \frac{-2\mathrm{i}y_c'(\tau)}{X^+(\tau)(\tau - z)}\mathrm{d}\tau. \tag{3.7}$$

Therefore, the solution for equation (3.6) is given by

$$\Phi_c(z) = -\frac{X(z)}{s}\int_{-1}^{1}\frac{y_c'(\tau)}{X^+(\tau)}\coth\left(\frac{\pi(\tau-z)}{s}\right)\,\mathrm{d}\tau. \tag{3.8}$$

(iii) Angle of Attack Term, Φ_α

We decompose (3.3) into parts depending only on angle of attack and write

$$\Phi_\alpha^+(t) + \Phi_\alpha^-(t) = 2\mathrm{i}\alpha, \tag{3.9}$$

which has the simple solution

$$\Phi_\alpha(z) = \mathrm{i}\alpha. \tag{3.10}$$

(b) Far-field behaviour

In this section we enforce that each solution decays at upstream infinity (V).

(i) Thickness term, Φ_{th}

Since $\coth(z) \to \pm 1$ as $z \to \pm\infty$, $\Phi_{th}(z) \to \pm\frac{1}{s}\int_{-1}^{1} y_{th}'(\tau)\mathrm{d}\tau = 0$ as $y_{th}(\pm 1) = 0$. Therefore, the upstream condition is already satisfied. Moreover, this result tells us that an unstaggered, thick cascade does not deflect a flow incident with zero angle of attack. This is what we would expect physically due to the symmetry of the problem, and we shall see later that this is not the case with non-zero angle of attack or camber.

(ii) Camber term, Φ_c

We note that

$$X(z) \to \mathrm{e}^{\mp\frac{\pi}{s}}, \tag{3.11}$$

as $z \to \pm\infty$. Applying this limit to (3.8) gives

$$\Phi_c(z) \to -\frac{\mathrm{e}^{\frac{\pi}{s}}}{s}\int_{-1}^{1}\frac{y_c'(\tau)}{X^+(\tau)}\,\mathrm{d}\tau,$$

as $z \to -\infty$. So the solution, in its current form, does not satisfy our upstream condition (V). We note that the boundary value problem defined by (I) and (II) is only unique up to the addition of a function holomorphic on $\mathbb{C}\setminus L$ that takes real values on $L^\pm$ and has the correct endpoint behaviour (III, IV). If we have such a function, then we can add an arbitrary multiple of it to the current solution and the resulting function will satisfy the same boundary value problem, albeit with modified far-field behaviour. An appropriate function is the fundamental solution, $X(z)$, which is pure imaginary on L. Addition of imaginary multiples of the fundamental solution will not affect the imaginary parts of the boundary values. Therefore, the modified function

$$\Phi_c(z) = -\frac{X(z)}{s}\int_{-1}^{1}\frac{y_c'(\tau)}{X^+(\tau)}\left(\coth\left(\frac{\pi(\tau-z)}{s}\right) - 1\right)\,\mathrm{d}\tau$$

now has the correct upstream behaviour.

(iii) Angle of attack, Φ_α

Similarly to the cambered case, we will use multiples of the fundamental solution to specify the correct upstream behaviour. The function with the correct upstream behaviour is

$$\Phi_\alpha(z) = \mathrm{i}\alpha\left(1 - X(z)\mathrm{e}^{-\frac{\pi}{s}}\right). \tag{3.12}$$

(c) Endpoint Behaviour

In this section, we verify that each solution posses the correct behaviour at the leading and trailing edges, according to (III, IV).

(i) Thickness term, Φ_{th}

The tangential velocity may be calculated by applying the Plemelj formula:

$$u_t^{\pm}(t) = -\frac{1}{s}\fint_{-1}^{1} y'_{th}(\tau)\coth\left(\frac{\pi(\tau-t)}{s}\right)\,\mathrm{d}\tau. \tag{3.13}$$

The tangential velocity is identical either side of the aerofoil and therefore the Kutta condition (IV) is satisfied. This can be seen by the symmetry of the problem and indicates that there will be no lift and therefore no flow deflection far downstream. As stated earlier, we only permit thickness functions whose derivatives have, at worst, square root singularities at the leading edge. This is certainly the case for aerofoils with parabolic leading edges, such as NACA aerofoils, where $y'_{th}(x) \sim x^{-1/2}$. We refer to Appendix B to explore the behaviour of our solution at the leading edge and show that it is consistent with condition (III). We write $f(t) = y'_{th}(t)$ for consistency with Appendix B. For the leading edge we have

$$f(t) = \frac{\tilde{f}(t)}{(t+1)^{1/2}},$$

where $\tilde{f}(t)$ satisfies a Hölder condition at $t=-1$. We apply equation (6.4c) so as $z \to -1 + \mathrm{i}ns$, with $z \notin L$,

$$\Phi_{th}(z) \sim \frac{\mathrm{e}^{\pi\mathrm{i}/2}}{2\mathrm{i}\sin(\pi/2)} \cdot \frac{\tilde{f}(-1)}{(z+1)^{1/2}} + \Phi_{t1}(z) + \Phi_{t0}(z).$$

Since $\Phi_{t0}(z)$ is bounded and tends to a definite limit as $z \to -1 + \mathrm{i}ns$, this corresponds to an inverse square root singularity, which is permissible. For the trailing edge, we have already established that the horizontal velocity jump is identically zero on the aerofoil and hence the Kutta condition is satisfied.

(ii) Camber term, Φ_c

We now use equation (3.6) and the Plemelj formulae (6.3) to give

$$u_c^{\pm}(t) = \mp\frac{X^+(t)}{s}\fint_{-1}^{1} \frac{y'_c(\tau)}{X^+(\tau)}\left(\coth\left(\frac{\pi(\tau-t)}{s}\right) - 1\right)\,\mathrm{d}\tau. \tag{3.14}$$

The Kutta condition states that the jump in horizontal velocity must be zero at the trailing edge, and this will only be the case if $u_c^{\pm}(1) = 0$. We apply the results of Appendix B, where

$$f(t) = \frac{y'_c(t)}{X^+(t)}.$$

We are in the case of equation (6.4d) where $\gamma = 1/2$, so

$$f(t) = \frac{\tilde{f}(t)}{(t-1)^{1/2}},$$

as $t \to 1$ where $\tilde{f}$ satisfies a Hölder condition at $t=1$. Therefore, as $t \to 1$ along the contour,

$$\Delta u_c(t) \sim -X^+(t)\left(\frac{\cot(\pi/2)}{2\mathrm{i}} \cdot \frac{\tilde{f}(1)}{(t-1)^{\gamma}} + \Phi_{c1}(t) + \Phi_{c0}(t)\right) = -X^+(t)\left(\Phi_{c1}(t) + \Phi_{c0}(t)\right) \to 0,$$

since $\Phi_{c0}(t)$ and $\Phi_{c1}(t)$ are bounded at $t=1$. Therefore, the Kutta condition is satisfied.

We now consider the behaviour at the leading edges. We are therefore in the case of equation (6.4a), with $f(t) = \tilde{f}(t)$, so as $z \to -1 + \mathrm{i}ns$, with $z \notin L$,

$$\Phi_c(z) \sim -X(z)\left(-\frac{f(-1)}{2\pi \mathrm{i}} \log\left(\frac{1}{z+1}\right) + \Phi_{c1}(z) + \Phi_{c0}(z)\right) = -X(z)\left(\Phi_{c1}(z) + \Phi_{c0}(z)\right).$$

Hence there is a square root singularity, which is permissible by (III).

(iii) Angle of attack, Φ_α

Clearly (3.12) has the correct endpoint behaviour and satisfied (III, IV). The tangential surface velocity is given by

$$u_\alpha^{\pm}(t) = \mp\alpha \mathrm{i} \mathrm{e}^{-\frac{\pi}{s}} X^+(t).$$

(d) Final Complex Velocity

By summing the constituent parts of the problem, we get

$$\Phi(z) = \mathrm{i}\alpha\left(1 - \mathrm{e}^{-\frac{\pi}{s}}\sqrt{\frac{\sinh\left(\frac{\pi(z-1)}{s}\right)}{\sinh\left(\frac{\pi(z+1)}{s}\right)}}\right) - \frac{1}{s}\int_{-1}^{1} y'_{th}(\tau)\coth\left(\frac{\pi(\tau - z)}{s}\right)\mathrm{d}\tau$$

$$- \frac{1}{\mathrm{i}s}\sqrt{\frac{\sinh\left(\frac{\pi(z-1)}{s}\right)}{\sinh\left(\frac{\pi(z+1)}{s}\right)}}\int_{-1}^{1} y'_c(\tau)\sqrt{\frac{\sinh\left(\frac{\pi(1+\tau)}{s}\right)}{\sinh\left(\frac{\pi(1-\tau)}{s}\right)}}\left(\coth\left(\frac{\pi(\tau - z)}{s}\right) - 1\right)\mathrm{d}\tau. \quad (3.15)$$

Due to the approximation of the staggered chord to a horizontal line in Section 2, the leading edge stagnation points are at $-1 + \mathrm{i}ns$ and the trailing edge stagnation points are at $+1 + \mathrm{i}ns$. We may include multiples of $\mathrm{e}^{\mathrm{i}\beta}$ in appropriate places to perturb these points to the correct locations ($-\mathrm{e}^{\mathrm{i}\beta} + \mathrm{i}ns$ for the leading edges and $\mathrm{e}^{\mathrm{i}\beta} + \mathrm{i}ns$ for the trailing edges) and only introduce $\mathcal{O}(\epsilon^2)$ errors. Therefore, the final solution for the complex potential with these singularities in the correct locations is given by

$$\Phi(z) = \mathrm{i}\alpha\left(1 - \mathrm{e}^{-\frac{\pi}{s}}\sqrt{\frac{\sinh\left(\frac{\pi(z-\mathrm{e}^{\mathrm{i}\beta})}{s}\right)}{\sinh\left(\frac{\pi(z+\mathrm{e}^{\mathrm{i}\beta})}{s}\right)}}\right) - \frac{1}{s}\int_{-1}^{1} y'_{th}(\tau)\coth\left(\frac{\pi(\tau\mathrm{e}^{\mathrm{i}\beta} - z)}{s}\right)\mathrm{e}^{\mathrm{i}\beta}\,\mathrm{d}\tau$$

$$- \frac{1}{\mathrm{i}s}\sqrt{\frac{\sinh\left(\frac{\pi(z-\mathrm{e}^{\mathrm{i}\beta})}{s}\right)}{\sinh\left(\frac{\pi(z+\mathrm{e}^{\mathrm{i}\beta})}{s}\right)}}\int_{-1}^{1} y'_c(\tau)\sqrt{\frac{\sinh\left(\mathrm{e}^{\mathrm{i}\beta}\frac{\pi(1+\tau)}{s}\right)}{\sinh\left(\mathrm{e}^{\mathrm{i}\beta}\frac{\pi(1-\tau)}{s}\right)}}\left(\coth\left(\frac{\pi(\tau\mathrm{e}^{\mathrm{i}\beta} - z)}{s}\right) - 1\right)\mathrm{e}^{\mathrm{i}\beta}\,\mathrm{d}\tau. \quad (3.16)$$

It should be noted that, in the asymptotic limit $s \to \infty$, this matches the well-known case of the flow around a single aerofoil [26].

4. Inverse Problem Solution

We now consider the problem where the tangential velocities on the upper and lower surfaces of the aerofoils are specified and an appropriate aerofoil geometry must be found. We may use equations (3.13) and (3.14) to find singular integral equations for the thickness, camber and angle

of attack:

$$-\frac{2}{s}\fint_{-1}^{1} y'_{th}(\tau)\coth\left(\frac{\pi(\tau-t)}{s}\right)\,\mathrm{d}\tau = u^{+}(t)+u^{-}(t), \tag{4.1}$$

$$-\frac{2X^{+}(t)}{s}\fint_{-1}^{1}\frac{y'_{c}(\tau)-\alpha}{X^{+}(\tau)}\left(\coth\left(\frac{\pi(\tau-t)}{s}\right)-1\right)\,\mathrm{d}\tau = u^{+}(t)-u^{-}(t). \tag{4.2}$$

where $u^{\pm}(t)$ each satisfy a Hölder condition on $(-1,1)$, except possibly at the end points, where they have, at worst, integrable singularities. We solve these equations separately.

(a) Inverse Problem – Thickness

We define the auxiliary function

$$I_{th}(z) = -\frac{1}{s}\int_{-1}^{1} y'_{th}(\tau)\coth\left(\frac{\pi(\tau-z)}{s}\right)\,\mathrm{d}\tau, \tag{4.3}$$

so that

$$I^{+}_{th}(t)+I^{-}_{th}(t) = u^{+}(t)+u^{-}(t).$$

This Riemann-Hilbert problem is analogous to the one stated in equation (3.6) and therefore has the solution

$$I_{th}(z) = \frac{X(z)}{2\mathrm{i}s}\int_{-1}^{1}\frac{u^{+}(t)+u^{-}(t)}{X^{+}(t)}\coth\left(\frac{\pi(\tau-z)}{s}\right)\,\mathrm{d}\tau. \tag{4.4}$$

Taking the difference either side of L and equating the expressions in (4.3) and (4.4) yields

$$y'_{th}(t) = \frac{X^{+}(t)}{2s}\fint_{-1}^{1}\frac{u^{+}(\tau)+u^{-}(\tau)}{X^{+}(\tau)}\coth\left(\frac{\pi(\tau-t)}{s}\right)\,\mathrm{d}\tau, \tag{4.5}$$

subject to the solvability condition

$$\int_{-1}^{1}\frac{u^{+}(\tau)+u^{-}(\tau)}{X^{+}(\tau)}\,\mathrm{d}\tau = 0. \tag{4.6}$$

This condition is necessary because it ensures that (4.3) matches (4.4) in the far-field. Moreover, it can be seen by integrating (4.5) that this condition guarantees that $y_{th}(-1)=y_{th}(+1)$. Physically, this condition can be viewed as a consequence of conservation of momentum; if (4.6) did not hold, then a non-lifting cascade would generate a non-zero deflection angle. In Section 5(c) we prove that this is not possible.

(b) Inverse Problem – Camber and Angle of Attack

Similarly to the previous section, we define the auxiliary function

$$I_{c,\alpha}(z) = -\frac{X(z)}{s}\int_{-1}^{1}\frac{y'_{c}(\tau)-\alpha}{X^{+}(\tau)}\left(\coth\left(\frac{\pi(\tau-z)}{s}\right)-1\right)\,\mathrm{d}\tau, \tag{4.7}$$

so that

$$I^{+}_{c,\alpha}(t)-I^{-}_{c,\alpha}(t) = u^{+}(t)-u^{-}(t).$$

This Riemann-Hilbert problem is the same as (3.2) and therefore has the solution, with correct far-field behaviour,

$$I_{c,\alpha}(z) = \frac{1}{2\mathrm{i}s}\int_{-1}^{1}\left(u^{+}(\tau)-u^{-}(\tau)\right)\left(\coth\left(\frac{\pi(\tau-z)}{s}\right)-1\right)\,\mathrm{d}\tau. \tag{4.8}$$

Taking the sum either side of L and equating the expressions in (4.7) and (4.8) yields

$$y_c'(t) - \alpha = \frac{1}{2s} \fint_{-1}^{1} \left(u^+(\tau) - u^-(\tau)\right) \left(\coth\left(\frac{\pi(\tau - t)}{s}\right) - 1\right) \mathrm{d}\tau. \tag{4.9}$$

In each case, the asymptotic behaviour indicates that the singularity at the trailing edge is, at worst, integrable and therefore the aerofoil shape can be found.

Both equations (4.5) and (4.9) may be substituted back into (4.1) and (4.2) respectively. By applying the Poincaré-Bertrand transformation formula [21, §23] it may be shown that the stated thickness, camber and angle of attack do, in fact, result in the correct velocity distributions.

5. Results

In this section we give details of some of the aerodynamically relevant results using the analysis of Section 3.

(a) Flow field

We may use (3.16) to plot the velocity fields and streamlines in figure 2. The streamlines show good agreement with the aerofoil surfaces and the flow leaves the aerofoils' trailing edges smoothly, indicating that the Kutta condition is satisfied. The flow perturbation is greatest near the leading and trailing edges, where singularities and stagnation points develop, and in the inter-blade region. Away from the cascade, the flow becomes uniform exponentially fast, in contrast to the single-aerofoil case, where the flow becomes uniform only algebraically fast.

(b) Tangential Surface Velocity

We may sum the tangential velocity distributions found in Section 3 to find the total distribution either side of each aerofoil:

$$\begin{aligned} u^{\pm}(t) = \pm\alpha \mathrm{e}^{-\frac{\pi}{s}} \sqrt{\frac{\sinh\left(\frac{\pi(1-t)}{s}\right)}{\sinh\left(\frac{\pi(1+t)}{s}\right)}} - \frac{1}{s} \fint_{-1}^{1} y_{th}'(\tau) \coth\left(\frac{\pi(\tau - t)}{s}\right) \mathrm{d}\tau \\ \mp \frac{1}{s} \sqrt{\frac{\sinh\left(\frac{\pi(1-t)}{s}\right)}{\sinh\left(\frac{\pi(1+t)}{s}\right)}} \fint_{-1}^{1} y_c'(\tau) \sqrt{\frac{\sinh\left(\frac{\pi(1+\tau)}{s}\right)}{\sinh\left(\frac{\pi(1-\tau)}{s}\right)}} \left(\coth\left(\frac{\pi(\tau - t)}{s}\right) - 1\right) \mathrm{d}\tau. \end{aligned} \tag{5.1}$$

In figure 3 we plot this tangential surface velocity as a function of distance along the chord for a variety of aerofoil spacings and geometries.

The analytical solution is compared with a numerical solution [5] which is obtained by using a conformal map to transform the cascade of aerofoils to a single object and the potential flow over this body is solved using a higher-order vortex panel method [19]. This numerical method has shown good agreement with other numerical [15] and experimental results [18]. In figure 3, the agreement between the analytic and numerical solutions is almost exact in the cases of angle of attack and camber and the only significant deviations occur at the leading edge of the thick aerofoils, where our assumption of small gradient breaks down. In order to resolve this, a further expansion in the $\mathcal{O}(\epsilon^2)$ region and asymptotic matching is required, but this is beyond the scope of the paper. The divergence from the numerical solution at the thick leading edge is also observed in the single aerofoil case at $\mathcal{O}(\epsilon)$. As verified by the asymptotic behaviour of the analytic solution close to the edges in Section 3(c), the Kutta condition can be seen to be satisfied since the tangential velocities match at the trailing edge and the leading edge has an integrable singularity. In the cases of angle of attack and camber, the tangential surface velocity is equal magnitude but opposite sign either side of the aerofoils, whereas in the thickness case the upper and lower velocities match.

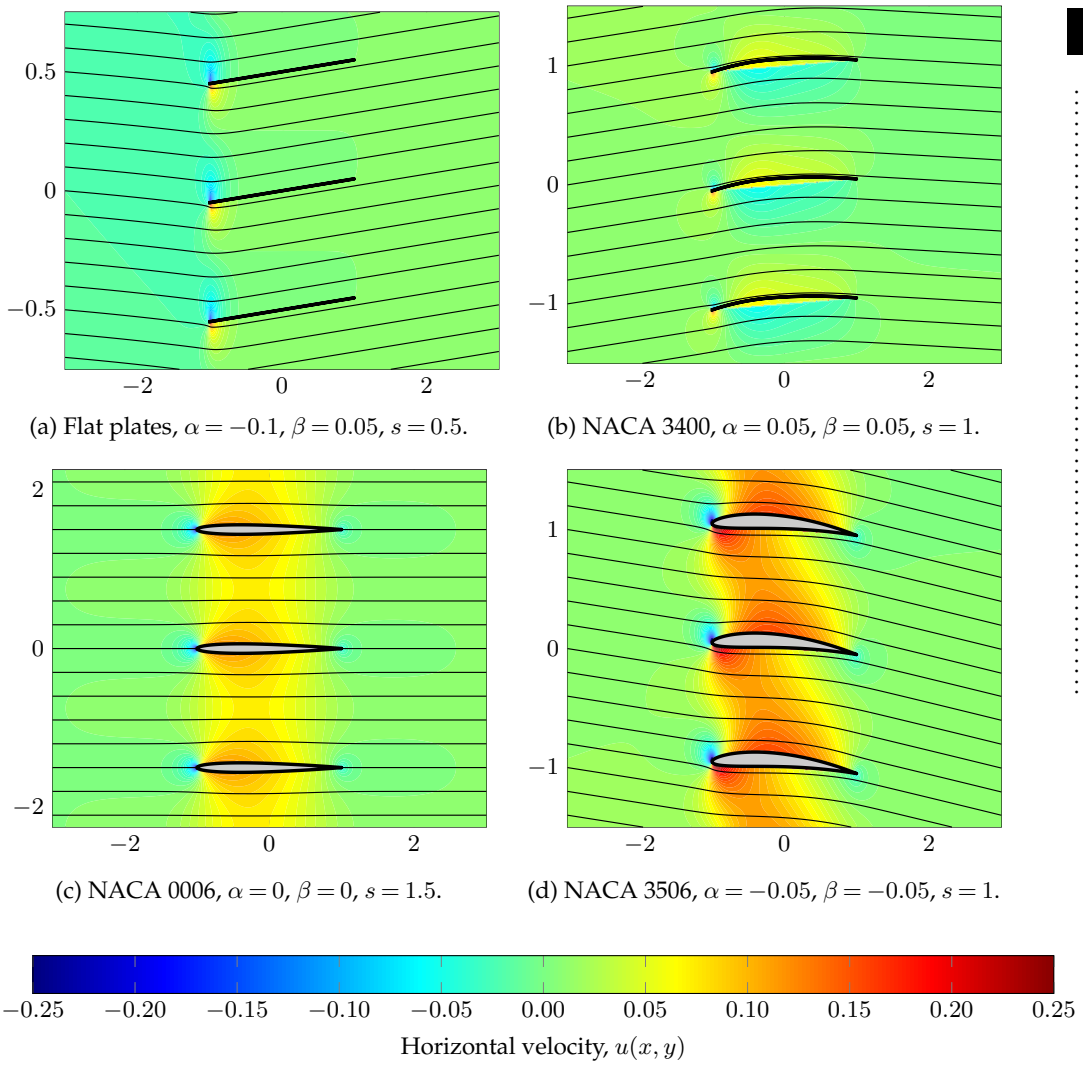

(a) Flat plates, $\alpha = -0.1$, $\beta = 0.05$, $s = 0.5$.

(b) NACA 3400, $\alpha = 0.05$, $\beta = 0.05$, $s = 1$.

(c) NACA 0006, $\alpha = 0$, $\beta = 0$, $s = 1.5$.

(d) NACA 3506, $\alpha = -0.05$, $\beta = -0.05$, $s = 1$.

Figure 2: Horizontal velocity and streamline plots for cascades of flat plates and three sets of NACA aerofoils. The streamlines are indicated in black and the background colour shows the horizontal velocity perturbation.

(c) Deflection Angle and Lift

A primary purpose of aerofoil cascades in aerodynamic applications is to deflect the flow through a desired angle. Our analysis allows us to derive an analytic expression for the change in flow angle, denoted by $\Delta\alpha$, for a given cascade geometry and inlet angle. Since the change in angle of attack is small, we have

$$\Delta\alpha = \mathrm{Im}\left[\overline{\Phi}(+\infty) - \overline{\Phi}(-\infty)\right] = -\Phi(+\infty).$$

We can use our expression for the flow perturbation (3.16) to write

$$\Delta\alpha = 2\mathrm{e}^{-\frac{\pi}{s}}\left\{-\alpha\sinh\left(\frac{\pi}{s}\right) + \frac{1}{s}\int_{-1}^{1} y_c'(\tau)\sqrt{\frac{\sinh\left(\frac{\pi(1+\tau)}{s}\right)}{\sinh\left(\frac{\pi(1-\tau)}{s}\right)}}\,\mathrm{d}\tau\right\}, \tag{5.2}$$

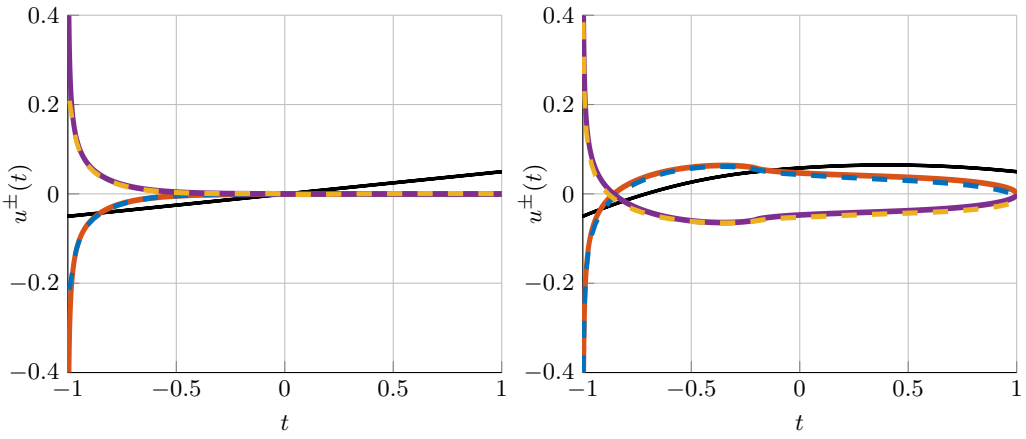

(a) Flat plates, $\alpha = -0.1$, $\beta = 0.05$, $s = 0.5$.

(b) NACA 3400, $\alpha = 0.05$, $\beta = 0.05$, $s = 1$.

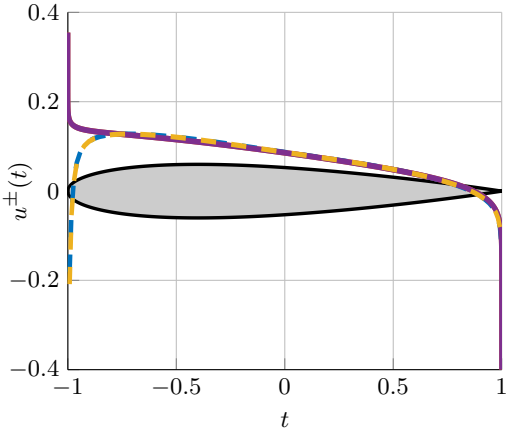

(c) NACA 0006, $\alpha = 0$, $\beta = 0$, $s = 1.5$.

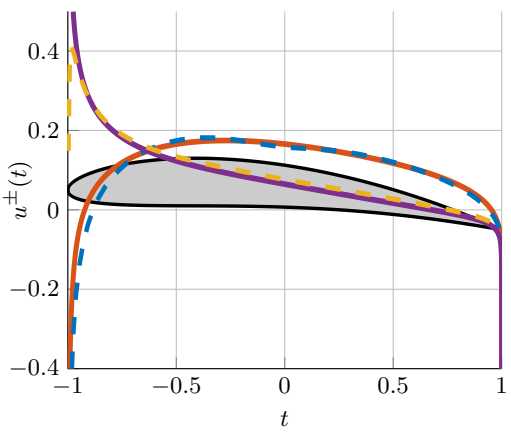

(d) NACA 3506, $\alpha = -0.05$, $\beta = -0.05$, $s = 1$.

Figure 3: Tangential surface velocity plots for flat plates and three sets of NACA aerofoils. Our analytical solution is given by the solid lines, corresponding to the upper and lower surfaces. The numerical solution is given by the dashed lines corresponding to the upper and lower surfaces.

where we have ignored $\mathcal{O}(\epsilon^2)$ terms for clarity. This equation may be used to choose the spacing, angle of attack or camber in order to achieve a desired deflection angle.

We may evaluate the deflection angle for the different limits of s: as the aerofoil spacing increases, $s \to \infty$, we have

$$\Delta\alpha \sim \frac{1}{s}\left(-2\pi\alpha + 2\int_{-1}^{1} y_c'(\tau)\sqrt{\frac{1+\tau}{1-\tau}}\right), \tag{5.3}$$

and the deflection angle decays algebraically as the aerofoil spacing increases. This is consistent with the single blade case [26] where there is no flow deflection far downstream of the blade. Conversely, if we consider the limit of very close blades, $s \to 0^+$, then

$$\Delta\alpha \sim -\alpha + y_c'(1).$$

The asymptotic behaviour of the integral in (5.2) is evaluated using Laplace's method. This equation states that the deflection angle will be equal to the difference between of the angle of

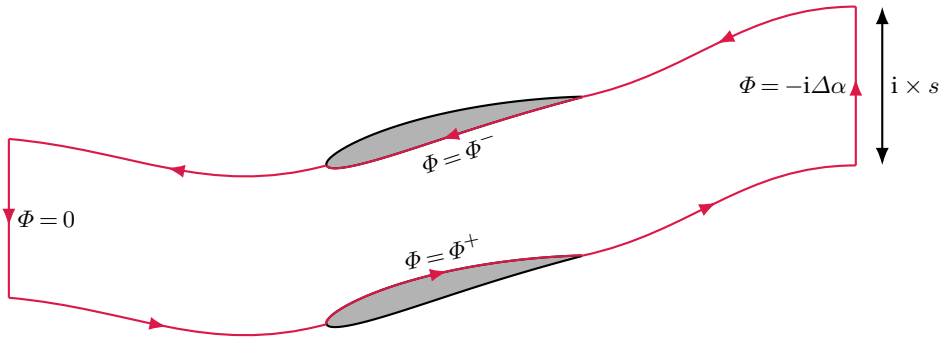

Figure 4: The contour of integration illustrating the relationship between circulation and deflection angle.

the trailing edge of the mean line of the aerofoil and the angle of attack. In other words, the outlet angle is the angle of the camber at the trailing edge.

The deflection angle is closely connected to the aerofoil lift; the Kutta-Joukowski theorem expresses the lift per unit span acting on the aerofoil as

$$\mathcal{L} = \rho_\infty U_\infty \Gamma. \tag{5.4}$$

The circulation is

$$\Gamma = \oint_C \boldsymbol{u} \cdot \mathrm{d}\boldsymbol{t} = \int_{-1}^{1} (\Phi^+(t) - \Phi^-(t))\mathrm{d}t = \int_{-1}^{1} \Delta u(t)\mathrm{d}t,$$

where Δu is given by equation (5.1). The integral is complicated to calculate, but may be evaluated analytically using residue calculus. However, this intricacy can be avoided by expressing the lift in terms of the deflection angle. To this end, we integrate Φ along an appropriate contour, as illustrated in figure 4.

This contour consists of the streamline corresponding to the upper surface of an aerofoil, the streamline corresponding to the lower surface of the aerofoil directly above, and two vertical contours at upstream and downstream infinity of length s. In this region, Φ is holomorphic and the resulting integral is zero by Cauchy's theorem. Due to the periodicity of Φ, the contributions from the streamlines cancel out except on the aerofoil surface, which corresponds to the circulation, Γ. The upstream vertical contribution vanishes and we are left with the downstream vertical contribution: $-\mathrm{i}\Delta\alpha \times \mathrm{i}s$. Rearranging the integral yields the expression

$$\Gamma = -s\Delta\alpha, \tag{5.5}$$

where the analytic expression of $\Delta\alpha$ is given in equation (5.2). Substituting (5.5) into (5.4) yields an analytic expression for the lift. This relation may be understood as a result of conservation of momentum; the net change in momentum (the change in flow angle times the aerofoil spacing) must be equal to the force exerted on the fluid (the lift). The single aerofoil result for the lift [26] may be recovered from (5.3) and (5.5). In this limit the deflection angle decays, but the lift approaches a constant value.

(d) Exact Analytical Solutions

Whilst the evaluation of the principal value integrals in (3.16) and (5.1) and their inversions (4.5, 4.9) must be done, in general, numerically to produce results such as figures 2 and 3, in some cases exact analytical evaluation is possible. This is useful to validate the solution to the inverse problem. For example, no integrals are required for flat plates with stagger and angle of

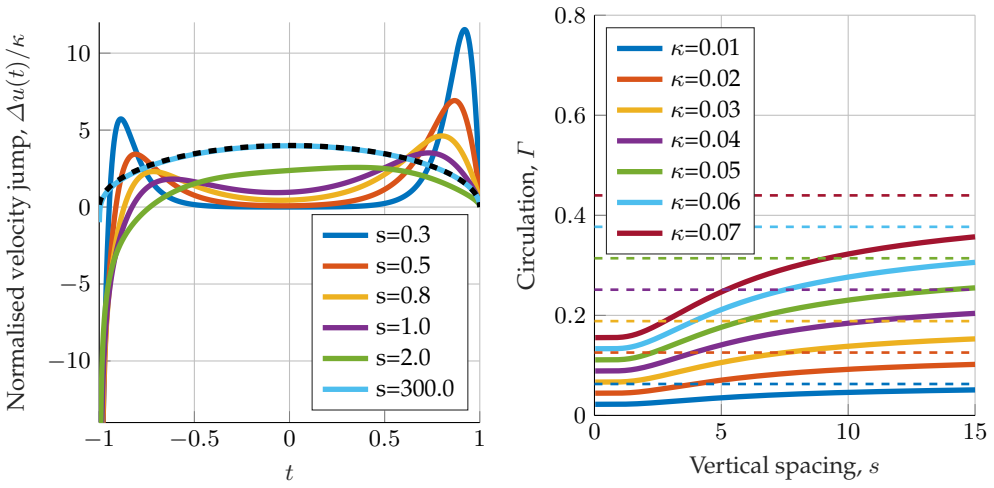

(a) The jump in tangential velocity as a function of distance along chord for a variety of aerofoil spacings.

(b) The circulation, Γ, as a function of aerofoil spacing, s, for a variety of almost-parabolic cambers.

Figure 5: Analytical calculations of aerodynamic properties for aerofoils with almost-parabolic camber (5.6). The single aerofoil case is given by the dashed lines and agrees with the asymptotic limit $s \to \infty$.

attack. Additionally, aerofoils with shape

$$y_b^{\pm}(t) = y_c(t) \pm y_{th}(t) = \kappa \frac{\tanh\left(\pi \frac{1+t}{s}\right) \tanh\left(\pi \frac{1-t}{s}\right)}{\tanh^2\left(\frac{\pi}{s}\right)}, \tag{5.6}$$

and no thickness, furnish analytical expressions. This shape approaches the parabolic camber distribution $y_c(t) = \kappa(1+t)(1-t)$ in the large s limit, and analytical expressions are also available in the single aerofoil case. The shape described in (5.6) can be thought of as the periodic analogy of this and it is chosen specifically to be analytic in the complex plane and appropriately periodic. This allows the integrals to be evaluated analytically using residue calculus; some mathematical details can be found in Appendix C. The original aerofoil shape can also be recovered from the tangential surface velocity distribution by the inversion formulae (4.5, 4.9). Values for the normalised tangential velocity jump and circulation can be observed in figures 5a and 5b and comparisons with the single aerofoil case are given by dashed lines.

6. Conclusions

We have adapted an existing method to analytically calculate the potential flow through an infinite cascade of aerofoils. Elements of this solution have been chosen to satisfy the appropriate edge conditions at the leading and trailing edges, as well as the correct upstream behaviour. Analytic expressions for the surface velocity, deflection angle, and lift have been calculated in terms of the angle of attack and aerofoil geometry and their asymptotic behaviour has been shown to match with well established results for single aerofoils. The expressions for surface velocity have been shown to agree well with numerical solutions which have been validated against experimental results.

The model and method of solution are readily extendable to a variety of situations. For example, the generalisation to weakly compressible flows is straightforward, and follows swiftly by a Prandl-Glauert transformation [19] provided the flow is not transonic. Also, multiple

cascades may be easily included in the analysis to model, for example, multiple columns of swimmers in shoals of fish. Having elucidated the kernel of the singular integral operator, it is now plain to see that the flow perturbation approaches uniformity exponentially fast away from the cascade unlike the single aerofoil case, where the flow becomes uniform algebraically quickly away from the blade. This means that we may place a second cascade almost directly behind the first one and, taking the angle of attack experienced by the second cascade from equation 5.2, calculate the new flow field. This can be performed for any number of cascades. Finally, a useful extension to the model in aeroacoustic applications would be to allow for porous aerofoils, where a similar approach to [16] may be applied.

Ethics. There are no ethical concerns in the paper.

Data Accessibility. All of the theoretical results can be generated from the equations provided in the paper.

Authors' Contributions. P. J. B. derived the mathematical model and its solution and generated and analysed the results. Both authors contributed to the writing of the manuscript and gave final approval for publication.

Competing Interests. We declare we have no competing interests.

Funding. This research was supported by an Engineering and Physical Sciences Research Council (EPSRC) award to P. J. B. from the University of Cambridge.

Acknowledgements. Professor Sheryl Grace and Dorien Villafranco contributed the numerical, vortex-method solution for the cascade which was developed as part of a project sponsored by the Aeroacoustics Research Consortium via the Ohio Aerospace Institute. P.J.B. also acknowledges the support of Jesus College, Cambridge, for the provision of funds for travel to conferences.

Appendices

A Modified Plemelj Formulae

In this section we prove the Modified Plemelj Formulae which is used in the solution of the Riemann-Hilbert problem in Section 3. The traditional Plemelj formulae must be adapted to be suitable for unbounded domains, as found in the cascade problem.

Theorem 6.1. *If $f(t)$ satisfies a Hölder condition on L as defined in Section 2, except possibly at the endpoints where it may have integrable singularities, and has period ins, then, for $z \notin L$,*

$$\Phi(z) := \frac{1}{2\pi i}\int_L \frac{f(\zeta)}{\zeta - z}\,d\zeta = \frac{1}{2is}\int_{-1}^{1} f(\tau)\coth\left(\frac{\pi(\tau - z)}{s}\right)\,d\tau. \tag{6.1}$$

Proof. By parametrising L, we may write

$$\frac{1}{2\pi \mathrm{i}}\int_L \frac{f(\zeta)}{\zeta - z}\,\mathrm{d}\zeta = \frac{1}{2\pi \mathrm{i}}\sum_{n=-\infty}^{\infty}\int_{-1}^{1}\frac{f(\tau)}{(\tau + \mathrm{i}ns) - z}\,\mathrm{d}\tau.$$

We now use the dominated convergence theorem to interchange the orders of summation and integration for $z \notin L$. We write

$$h_N(\tau, z) := f(\tau)\sum_{n=-N}^{N}\frac{1}{(\tau + \mathrm{i}ns) - z} = f(\tau)\left(\frac{1}{\tau - z} + 2\sum_{n=1}^{N}\frac{(\tau - z)}{(\tau - z)^2 + n^2 s^2}\right),$$

and then

$$|h_N(\tau, z)| \le g(\tau, z) := |f(\tau)|\left(\frac{1}{|\tau - z|} + 2\sum_{n=1}^{\infty}\frac{|(\tau - z)|}{|(\tau - z)^2 + n^2 s^2|}\right). \tag{6.2}$$

To complete the proof, we must show that g is integrable. As f satisfies the Hölder condition and possibly has integrable singularities at the end points, all that remains is to show that the bracketed term is bounded. Since $z \notin L$, we may write $z - \tau = re^{i\theta}$, where r and θ are functions of τ. Moreover, $re^{i\theta} \neq \pm ins$ and therefore,

$$g(\tau, z) = \frac{|f(\tau)|}{r}\left(1 + 2\frac{r^2}{s^2}\sum_{n=1}^{\infty}\frac{1}{\left|\frac{r^2}{s^2}e^{2i\theta} + n^2\right|}\right).$$

By the comparison test with $\frac{1}{n^2}$, this sum converges for all $\tau \in [-1, 1]$, so $g(\tau, z)$ is bounded in the domain of integration and therefore integrable. By the dominated convergence theorem, we are free to interchange the order of limit and integral, so

$$\frac{1}{2\pi i}\int_L \frac{f(\zeta)}{\zeta - z}\,d\zeta = \frac{1}{2\pi i}\int_{-1}^{1} f(\tau)\sum_{n=-\infty}^{\infty}\frac{1}{(\tau + ins) - z}\,d\tau = \frac{1}{2is}\int_{-1}^{1} f(\tau)\coth\left(\frac{\pi(\tau - z)}{s}\right)d\tau,$$

where the last identity is obtained from a formula in [7, p. 296]. □

Since, as we have shown above, we may split up the integral into its contributions from each chord, we have

$$\frac{1}{2\pi i}\int_L \frac{f(\zeta)}{\zeta - z}\,d\zeta = \frac{1}{2is}\int_{-1}^{1} f(\tau)\coth\left(\frac{\pi(\tau - z)}{s}\right)d\tau,$$

and the analogous result for the Plemelj formulae holds:

$$\Phi^{\pm}(t) = \pm\frac{f(t)}{2} + \frac{1}{2is}\int_{-1}^{1} f(\tau)\coth\left(\frac{\pi(\tau - t)}{s}\right)d\tau. \tag{6.3}$$

B Asymptotic results at endpoints

In this section, we consider the asymptotic behaviour of Cauchy-type integrals with coth kernels, which is necessary for the analysis of endpoint behaviour in Section 3(c). We restrict our attention to the endpoints ± 1, since the behaviour at $\pm 1 + ins$ will be identical by the periodicity of the kernel. We define

$$\Phi(z) = \frac{1}{2is}\int_{-1}^{1} f(\tau)\coth\left(\frac{\pi(\tau - z)}{s}\right)d\tau = \Phi_1(z) + \frac{1}{2\pi i}\int_{-1}^{1}\frac{f(\tau)}{\tau - z}d\tau, \tag{6.4}$$

where $f(t)$ satisfies a Hölder condition on $(-1, 1)$, except possibly at the ends where it satisfies

$$f(t) = \frac{\tilde{f}(t)}{(t - c)^{\gamma}},$$

where $c = \pm 1$, γ is a real constant, and $\tilde{f}(t)$ satisfies a Hölder condition near and at c. In our case the relevant parameters are $\gamma = 0, 1/2$. We have removed the principal value part in (6.4) so that Φ_1 is bounded and takes a definite value as $z \to c$ along any path. When $z = t$ on the contour, the remaining integral is considered in the principal value sense. In the following formulae, $\pm$ correspond to taking $c = \pm 1$. Additionally, the function $\Phi_0(z)$ is also bounded and tends to a definite limit as $z \to c$ along any path. The function $\Psi_0(t)$ satisfies a Hölder condition near c. The branch of $\log\frac{1}{z-c}$ is chosen to pass through the contour. Then the following limits, which can be deduced from [21, §29], are valid:

(i) $\underline{\gamma = 0}$

(a) As $z \to c$, with z not on the contour

$$\Phi(z) \sim \pm\frac{f(c)}{2\pi i}\cdot\log\left(\frac{1}{z - c}\right) + \Phi_1(z) + \Phi_0(z). \tag{6.4a}$$

(b) As $t \to c$, with t on the contour

$$\Phi(t) \sim \pm \frac{f(c)}{2\pi \mathrm{i}} \cdot \log\left(\frac{1}{t-c}\right) + \Phi_1(t) + \Psi_0(t). \tag{6.4b}$$

(ii) $\underline{\gamma \neq 0}$

(a) As $z \to c$, with z not on the contour

$$\Phi(z) \sim \pm \frac{\mathrm{e}^{\pm\gamma\pi\mathrm{i}}}{2\mathrm{i}\sin(\gamma\pi)} \cdot \frac{\tilde{f}(c)}{(z-c)^{\gamma}} + \Phi_1(z) + \Phi_0(z). \tag{6.4c}$$

(b) As $t \to c$, with t on the contour

$$\Phi(t) \sim \pm \frac{\cot(\gamma\pi)}{2\mathrm{i}} \cdot \frac{\tilde{f}(c)}{(t-c)^{\gamma}} + \Phi_1(t) + \Psi_0(t). \tag{6.4d}$$

C Exact Analytical Solutions

In this section we give some details of the exact analytical solutions for the aerofoils with geometry given by (5.6). This choice of camber is chosen specifically to allow the analytical calculation of surface velocity distribution and circulation. After manipulation, the camber gradient is given by

$$y_c'(t) = -\kappa \frac{\pi}{s} \cdot \frac{\cosh\left(\frac{2\pi}{s}\right)}{\tanh^2\left(\frac{\pi}{s}\right)} \cdot \operatorname{sech}^2\left(\pi \frac{1-t}{s}\right) \operatorname{sech}^2\left(\pi \frac{1+t}{s}\right) \sinh\left(2\pi \frac{t}{s}\right). \tag{6.5}$$

By using residue calculus, we may apply equation (5.1) and calculate the surface velocity distribution. The integral around the branch cut (which is twice integral we are trying to calculate) may be deformed to an indented rectangle of height s and length $2R$, as illustrated in figure 6. This deformation can be used when the integral is taken in a principal value sense and there is a non-integrable singularity on the branch cut. As $R \to \infty$, the vertical contributions vanish. The periodicity of the integrand means that contributions from the horizontal sides cancel except from the contributions due to poles at $t = -1 \pm \mathrm{i}s/2,\ 1 \pm \mathrm{i}s/2$. By summing the residues obtained by traversing these poles clockwise, we obtain the expression for the jump in tangential velocity

$$\Delta u(t) = -\kappa \frac{\pi \mathrm{i}}{s} X^+(t) \coth^2\left(\frac{\pi}{s}\right) \times \left(\frac{\tanh\left(\pi\frac{1-t}{s}\right) + 2\coth\left(\frac{2\pi}{s}\right)\operatorname{sech}^2\left(\pi\frac{1-t}{s}\right) - 1}{\sqrt{\operatorname{sech}\left(\frac{2\pi}{s}\right)}} + \frac{\tanh\left(\pi\frac{1+t}{s}\right) - 2\coth\left(\frac{2\pi}{s}\right)\operatorname{sech}^2\left(\pi\frac{1+t}{s}\right) + 1}{\sqrt{\cosh\left(\frac{2\pi}{s}\right)}} \right). \tag{6.6}$$

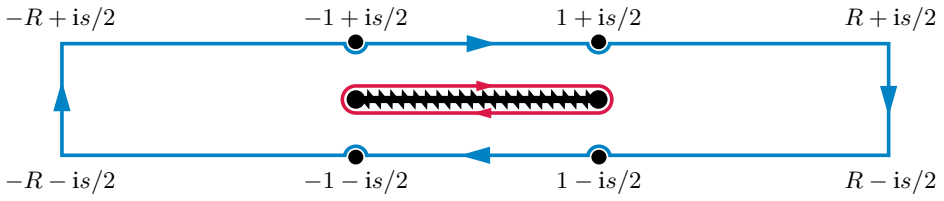

Figure 6: The contour of integration for the almost-parabolic camber distribution in the complex τ-plane. The red line represents the integral around the branch cut and the blue line represents the deformed contour.

We may now invert this to retrieve the original aerofoil shape. The solvability condition (4.6) is satisfied since the sum of velocity either side of the blade is zero. Substituting (6.6) back into (4.9) and performing the contour integral according to figure 6 retrieves the original camber distribution (6.5).

Furthermore, we may analytically calculate the lift on a given aerofoil by using equations (5.2) and (5.5). The integral in this expression may be evaluated analytically, again using the method in figure 6 even though the integrand is slightly different, to get

$$\mathcal{L}' = \rho_\infty U_\infty \cdot 2\pi\kappa \mathrm{e}^{-\frac{\pi}{s}} \cosh^2\left(\frac{\pi}{s}\right) \sqrt{\operatorname{sech}\left(\frac{2\pi}{s}\right)}.$$

References

1. I. H. Abbott and A. E. Von Doenhoff, *Theory of Wing Sections: Including a Summary of Airfoil Data*, vol. 11, Dover Publications, 1959.
2. M. J. Ablowitz and A. S. Fokas, *Complex Variables: Introduction and Applications*, Cambridge University Press, 2003.
3. T. F. Balsa, *Potential Flow Interactions in an Array of Cylinders in Cross-Flow*, Journal of Sound and Vibration, 50 (1977), pp. 285–303.
4. G. K. Batchelor, *An Introduction to Fluid Dynamics*, Cambridge University Press, 2000.
5. A. Bhimarasetty and R. N. Govardhan, *A Simple Method for Potential Flow Simulation of Cascades*, Sadhana, 35 (2010), pp. 649–657.
6. H. Brenner, *Dispersion Resulting from Flow through Spatially Periodic Porous Media*, Philos. Trans. R. Soc. A Math. Phys. Eng. Sci., 297 (1980), pp. 81–133.
7. T. J. I. Bromwich, *An Introduction to the Theory of Infinite Series*, American Mathematical Soc., 2005.
8. L. J. Clancy, *Aerodynamics*, Wiley, 1978.
9. D. G. Crowdy, *Uniform flow past a periodic array of cylinders*, European Journal of Mechanics, B/Fluids, 56 (2016), pp. 120–129.
10. I. Evers and N. Peake, *On sound generation by the interaction between turbulence and a cascade of airfoils with non-uniform mean flow*, Journal of Fluid Mechanics, 463 (2002), pp. 25–52.
11. A. F. O. Falcão, *Three-dimensional potential flow through a rectilinear cascade of blades*, Ingenieur-Archiv, 44 (1975), pp. 27–41.
12. A. S. Fokas, *A Unified Approach to Boundary Value Problems*, Society for Industrial and Applied Mathematics, 2008.
13. F. D. Gakhov, *Boundary Value Problems*, Pergamon Press, 1966.
14. A. W. Goldstein and M. Jerison, *Isolated and Cascade Airfoils with Prescribed Velocity Distribution*, tech. rep., NACA, 1947.
15. J. P. Gostelow, *Cascade Aerodynamics*, Pergamon Press, 1 ed., 1984.
16. R. Hajian and J. W. Jaworski, *The Steady Aerodynamics of Aerofoils with Porosity Gradients*, Proceedings of the Royal Society A: Mathematical, Physical and Engineering Science, 473 (2017).
17. M. Hall and B. Thwaites, *On the Calculation of Cascade Flows*, tech. rep., Aeronautical Research Council, 1965.
18. L. Herrig, J. Emery, and J. Erwin, *Systematic Two-Dimensional Cascade Tests of NACA 65-series Compressor Blades at Low Speeds*, tech. rep., NASA, 1957.
19. A. M. Kuethe and C.-Y. Chow, *Foundations of Aerodynamics: Bases of Aerodynamic Design*, Wiley, 5 ed., 1998.
20. J. C. Liao, *A Review of Fish Swimming Mechanics and Behaviour in Altered Flows*, Philos. Trans. R. Soc. Lond. B. Biol. Sci., 362 (2007), pp. 1973–1993.
21. N. I. Muskhelishvili, *Singular Integral Equations: Boundary Problems of Function Theory and their Application to Mathematical Physics*, Dover Publications, 1946.
22. A. Robinson and J. A. Laurmann, *Wing Theory*, Cambridge University Press, 1956.
23. J. Schulten, *Sound Generated by Rotor Wakes Interacting with a Leaned Vane Stator*, AIAA Journal, 20 (1982), pp. 1352–1358.
24. R. A. Spurr and H. J. Allen, *A theory of unstaggered airfoil cascades in compressible flow*, National Advisory Committee for Aeronautics, NACA, (1947), p. 14.
25. T. Theodorsen and I. E. Garrick, *General Potential Theory of Arbitrary Wing Sections*, Tech. Rep. December, NASA, 1979.
26. B. Thwaites, *Incompressible Aerodynamics: an Account of the Theory and Observation of the Steady Flow of Incompressible Fluid Past Aerofoils, Wings, and Other Bodies*, Dover Publications, 1960.